https://doi.org/10.48048/tis.2024.7871

Facile Synthesis of Tin (II) Sulphate using Precipitation Method: Effect on Sulfuric Acid Concentration, Heating Temperature and Time, and Effect of Oxygen

Cherly Firdharini[1,2*], Yoki Yulizar[1], Agus Sukarto Wismogroho[2] and Wahyu Bambang Widayatno[2]

[1]Department of Chemistry, Mathematics and Sciences Faculty, Universitas Indonesia, Depok 16424, Indonesia
[2]Research Center for Advanced Material, National Research and Innovation Agency of Indonesia, Tangerang Selatan 15314, Indonesia

([*]Corresponding author's e-mail: cfirdharini96@gmail.com)

Received: 21 December 2023, Revised: 28 February 2024, Accepted: 7 March 2024, Published: 10 June 2024

Abstract

Exploring new methods and protocols for synthesizing tin (II) sulfate ($SnSO_4$) with low energy and time consumption is of significant industrial importance. We have developed synthesis protocols involving critical parameters, such as oxygen gas flow, sulfuric acid concentration and heating temperature dan time, aimed at yielding a high purity of $SnSO_4$ precipitate. Our findings indicate that oxygen gas flow significantly enhances the synthesis process, resulting in a high yield of pure $SnSO_4$ precipitate. The optimal synthesis conditions were identified as 180 °C for 2 h under continuous oxygen gas flow. This research shows the most efficient synthesis time rather than any prior research. Under these conditions, an intermediate oxide formed, which subsequently reacted with 30 %wt sulfuric acid to produce the desired yellowish $SnSO_4$ precipitate. The presence of tin (II) in the synthesized product was confirmed by the iodine test. Differential Thermal Analysis (DTA) was employed to analyze the product's thermal stability. X-ray Diffraction (XRD) analysis revealed a single-phase $SnSO_4$ crystal structure with an average particle size of 666 nm. Additionally, X-ray Fluorescence (XRF) analysis confirmed the product's purity, showing a tin (II) sulfate content of 98.369 %. Further studies using the Field-Emission Scanning Electron Microscope (FESEM) with Energy Dispersive X-Ray Spectroscopy (EDS) and Transmission Electron Microscope (TEM) confirmed the prismatic particle shape morphology of the $SnSO_4$ crystals, with an average size of 3.473 μm. The developed synthesis protocol provides a facile and energy-efficient approach to synthesize pure $SnSO_4$ material.

Keywords: Tin (II) sulfate ($SnSO_4$), High-purity synthesis, Precipitations, Oxygen effect

Introduction

Tin (Sn) holds immense value in various industrial applications, owing to its unique physical and chemical properties [1]. Among the many derivatives of tin, tin (II) sulfate ($SnSO_4$) stands out as a versatile material with a broad spectrum of applications. Its applications include transparent semiconductor oxide (TSO) for electronic devices [2], electrolyte additive for lead-acid batteries [3], anode material for lithium batteries [4], electrolyte for tin plating [1], anodized aluminum panels for solar water heating systems [5], precursor for SnO_2 synthesis [6] and catalyst for biodiesel production [7-9], among others. Given its widespread use, numerous methodologies have been thoroughly investigated to synthesize $SnSO_4$efficiently, focusing on minimizing energy consumption, synthesis duration and overall cost-effectiveness to attain high-purity $SnSO_4$.

To date, various physical and chemical methods have been employed to synthesize $SnSO_4$, including precipitation [10], electrochemical methods [11,12], substitution methods [10,13,14], in situ deposition methods [15], sol-gel methods [16] and others. Among these methods, the conventional precipitation method stands out as the most suitable approach, as it consumes less energy and time for $SnSO_4$ synthesis while producing minimal contaminants. In $SnSO_4$ synthesis, sulfuric acid is rarely utilized as the sulfate ion source. Instead, sulfate salts like copper (II) sulfate ($CuSO_4$) [14] and ammonium sulfate ($(NH_4)_2SO_4$) [15], are more commonly employed. However, prior studies have indicated that the most efficient method for synthesizing high-purity tin (II) sulfate ($SnSO_4$) utilizes tin metal as the precursor and sulfuric acid

[10,17,18]. However, these studies did not comprehensively delve into the chemical reactions involved in the formation of $SnSO_4$, nor did they thoroughly explore the factors that influence these reactions.

Previous research indicates that tin oxide (SnO) serves as a crucial intermediate compound in the synthesis of $SnSO_4$. Therefore, controlling the transformation of the tin precursor into SnO is expected to facilitate the formation of $SnSO_4$. This can be achieved using a precipitation method where the precursor is exposed to oxygen to form SnO intermediates, then reacted with sulfuric acid (H_2SO_4) and finally washed with distilled water and acetone. This approach is anticipated to emerge as the most environmentally friendly method for synthesizing $SnSO_4$ under elevated temperatures [19].

In terms of the reaction mechanism, molecular oxygen exposure initiates the oxidation process through the dissociation of oxygen molecules and the subsequent binding of atomic oxygen to surface atoms (dissociative chemisorption) [20-22]. Trapped at the metal surface, the precursor can either desorb into the gas phase or undergo dissociative chemisorption, with the relative rates determined by a kinetic competition governed by the surface temperature [22-25]. If not desorbed, the 2nd step involves the activated transition of the precursor to the chemisorbed atomic oxygen state, where the O-O bond is disrupted and the O atoms approach closer to the metal surface [22]. The oxygen rate constant can be considered as an approximate indicator of the dissolution rate of oxygen into sulfuric acid solution under oxidation reaction. The dissolution rate of oxygen into sulfuric acid solution decreases rapidly with increasing sulfuric acid concentration [26].

As tin exhibits passivity towards the following 5 acids: Sulfuric acid, hydrochloric acid, hydrobromic acid, hydroiodic acid and hexafluorosilicic acid [27], tin powder reacts with 50 - 95 % wt H_2SO_4 to yield $SnSO_4$ after heating for 5 - 30 days [10]. The concentration of H_2SO_4 and reaction temperature play a critical role in enhancing the tin dissolution process, thereby improving reaction efficiency [27]. Therefore, it is essential to determine the optimum sulfuric acid concentration, reaction temperature, reaction time and the effect of oxygen on the reaction. Additionally, the physical and chemical properties of the synthesized $SnSO_4$ and its kinetic studies were investigated in detail.

Materials and methods

Materials

The basic materials used in this paper included Tin powder which is powderized from Bankaesa tin bar casting (Sn 99.9999 %) and was provided by PT. Timah Industri, sulfuric acid (H_2SO_4) (AR 96.01 %) was procured from Mallinckrodt, Iodine, Potassium Iodide and Sodium thiosulphate were obtained from Merck, Pro analysis Tin (II) sulphate standard was acquired from Unilab, a technical grade oxygen gas with >98 % purity and distilled water.

Methods

Synthesis of Tin (II) sulphate ($SnSO_4$)

The method of $SnSO_4$ synthesis is adapted from previous research and modified in several parameter [10], such as concentration of sulfuric acid (under 50 %wt), heating temperature (more than 95 °C) and heating time (less than a day). The synthesis is followed by reacting 5.5289 g tin and oxygen with an oxygen flow of 15 mL/s for 12 min in the chamber. It was then dissolved with diluted H_2SO_4 solution (30, 35 and 40 %wt) and heated at 120, 150, 180 and 200 °C for 1, 2, 3, 4, 5 and 6 h. $SnSO_4$ precipitate was then separated from the solution using vacuum filtration and washed using cold water and acetone. The precipitation is dried afterward in oven at 110 °C and $SnSO_4$ powder is obtained.

Oxygen role in Tin (II) sulphate synthesis

The method of $SnSO_4$ synthesis includes the steps of reacting tin and oxygen with an oxygen flow of 15 mL/s for 12 min in the chamber. It was then reacted with the optimum concentration of sulfuric acid solution and heated using the optimum heating temperature for the optimum heating time. The resulting white-yellowish $SnSO_4$ precipitate then separated from the solution using vacuum filtration and washed using cold water and ethanol. The precipitation is dried afterward and $SnSO_4$ powder is obtained. For a blank, the synthesis method is carried out as describe above but without additional oxygen added to the chamber.

Characterization

The oxidation state of tin in each synthesized product is investigated using the classical qualitative analysis test by Iodine discoloration test [reduction of $I_{2(aq)}$ to $I^-_{(aq)}$ on oxidation of $Sn^{2+}_{(aq)}$ to $Sn^{4+}_{(aq)}$]. In addition, the thermal evolution of the material and the enthalpy process and the endothermic area of powder

synthesized were performed by Differential Thermal Analysis (DTA) of P2F type. This DTA test was run in a heating room that consisted of air gas, with a temperature of 30 to 1,000 °C, with a heating rate of 2.5 °C/min and alumina powder as a reference tube. The method has been calibrated using alumina with a temperature of 30 to 1,100 °C, with a heating rate of 2 - 10 °C/min. $SnSO_4$ which synthesized under optimum condition is tested using X-Ray Diffraction (XRD), X-ray Fluorescence (XRF) Field-Emission Scanning Electron Microscope - Energy Dispersive X-Ray Spectroscopy (FESEM-EDS) and Transmission Electron Microscope (TEM). XRD Rigaku Smartlab with A-26 CuKα X-ray tube was used to observe the diffraction pattern of $SnSO_4$. The setting of the XRD measurement was a step width of 0.01 degrees, a scan speed of 5.0985 degrees per minute, a range of 0 - 110 degrees, a voltage of 40 kV and a current of 30 mA. FESEM-EDS Jeol JIB-4610F type was used to observe the morphology, particle shape and semi-quantitative element of the powder product. TEM micrographs were acquired with a TEM Talos F200X is a type of TEM that uses X-FEG (high brightness) as an electron source with an accelerating voltage that can currently work at 80 and 200 kV.

Results and discussion

Reactor assembling

The reactor, constructed from corrosion-resistant Pyrex material, is meticulously sealed to maintain a controlled environment during the synthesis process, which involves concentrated strong acid and high temperatures. The reactor's design, as depicted in **Figure 1**, positions it atop the $MoSi_2$ heater system (1) as the primary heat source. To prevent gas leakage and ensure a stable reaction environment, each connector is meticulously sealed with high-temperature red sealant. The Pyrex reactor itself comprises a 3-neck flask serving as the synthesis chamber (2). The left side of the flask neck accommodates a thermocouple (3) that continuously monitors the real-time temperature, ensuring that the synthesis proceeds at the desired temperature without fluctuations. The right side of the neck is connected to a tube from a peristaltic pump (4), which precisely controls the oxygen flow rate from the oxygen gas cylinder (5). This precise oxygen replenishment is crucial for the synthesis reaction to proceed efficiently.

Three condensers (6, 7 and 8) are strategically positioned to effectively condense the vapor generated during the synthesis process. This condensation step is essential to recapture the vaporized materials and return them to the liquid state. The condensed liquid is collected in a secondary 3-neck flask (9), where the left neck (10) is connected to a hose to facilitate liquid suction and recirculation within the main synthesis chamber. Conversely, the right neck (11) is linked to a hose to direct the remaining gas into the Erlenmeyer reservoir (12), where NaOH solution acts as an absorber for any residual SO_x gas. The arrows in **Figure 1** visually represent the flow dynamics: The blue arrow depicts the movement of steam generated during the synthesis, the red arrow indicates the incoming oxygen flow and the green arrow traces the exhaust gas movement towards the NaOH absorber.

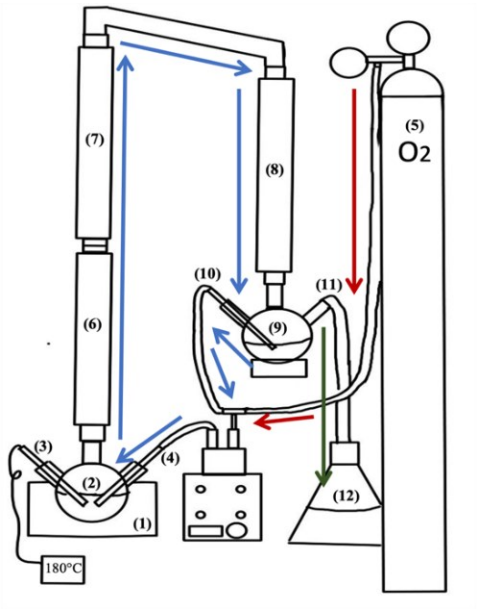

Figure 1 Scheme of $SnSO_4$ reactor.

Effect of sulfuric acid concentration on the synthesis of Tin (II) sulphate ($SnSO_4$)

Tin, a passive metal, exhibits resistance to dissolving in oxidizing acids [13], including sulfuric acid, hydrochloric acid, hydrobromic acid, hydroiodic acid and hexafluorosilicic acid [27]. However, it can be oxidized by oxygen [13-15] to form tin (II) oxide (SnO). Following the saturation of the reactor with oxygen, tin undergoes oxidation [12], gradually forming a thin, white SnO layer. As per Richter *et al.*, this layer represents an intermediate state, as described by the following reaction equation [9]:

$$2\ Sn_{(s)} + O_{2(g)} \rightarrow 2\ SnO_{(s)} \quad (1)$$

Oxygen is supplied to the tin powder as the synthesis process relies on its presence. Tin is oxidized by oxygen [28], leading to the formation of tin oxide (SnO) [18]. Mori et al. asserted [28] that pure tin does not readily dissolve in the absence of an oxidizing acid; however, Sn^{2+} ions can be generated when tin is dissolved in oxygen-saturated sulfuric acid [27-29]. These Sn^{2+} ions gradually undergo oxidation by oxygen, forming white deposits on the surface of the tin metal, akin to their formation from SnO by air oxidation [28].

After the formation of a thin white layer, the tin is ready for dissolution in sulfuric acid. Sulfuric acid solutions with varying concentrations (30, 35 and 40 wt.%) were introduced into the system. Throughout this process, oxygen continued to flow into the reaction chamber. Moreno et al. reported that SnO is an unstable compound in the absence of oxygen flow [30]. Therefore, to prevent disproportionation, oxygen is maintained in the chamber during the synthesis process. The disproportionation reaction depicted in Eq. (12) is spontaneous, indicated by minus in $\Delta G°$ [30]:

$$2\ SnO_{(s)} \rightarrow SnO_{2(s)} + Sn_{(s)} \qquad \Delta G° = -5.9\ kJ\ mol^{-1} \quad (2)$$

Once sulfuric acid is introduced into the reaction chamber, the heater is turned on and the temperature is set to 180 °C for 2 h. During the initial 30 min, tin reacts with 40 % sulfuric acid to form a yellowish-white solution compared to 35 and 30 % solutions. The overall reaction between tin and sulfuric acid is slow. This is because tin tends to exhibit passivity when reacting with sulfuric acid [27]; however, after the intermediate compound, SnO, is formed, the reaction that occurs within the chamber follows the following equation:

$$SnO_{(s)} + H_2SO_{4(aq)} \rightarrow SnSO_{4\ (s)} + H_2O_{\ (l)} \quad (3)$$

Those chemical reactions have yielded white, hygroscopic $SnSO_4$ powder, as depicted in **Figure 2**. Due to the hygroscopic nature of $SnSO_4$, it was stored in vacuum vials to maintain product quality [10]. The $SnSO_4$ powder of various concentrations was then subjected to qualitative iodine test and Differential Thermal Analysis (DTA) to determine its oxidation state.

Figure 2 Synthesized $SnSO_4$ powder.

Initial characterization of the synthesized $SnSO_4$ was performed using conventional iodine oxidation analysis. The discoloration iodine test is a qualitative test based on the oxidation-reduction reaction. Iodine (I_2) from the brown iodine solution will oxidize Sn^{2+} ions from $SnSO_4$ to form white iodide anions (I^-),

indicating the presence of Sn^{2+} ions in the synthesized powder. The reaction in the iodine test is represented by the following equation [10,31]:

$$I_{2\,(aq)} + Sn^{2+}{}_{(aq)}\,(\text{Brown Solution}) \rightarrow 2I^{-}{}_{(aq)} + Sn^{4+}{}_{(aq)}\,(\text{White Solution}) \quad (4)$$

The synthesized powders of 3 different sulfuric acid concentrations were each weighed and subjected to iodine test, yielding significant color variations. Powder synthesized using 30 % sulfuric acid produced a white solution (**Figure 3(a)**), indicating the presence of Sn^{2+} ions in the synthesized $SnSO_4$. The iodine test solution for powder produced at 35 % sulfuric acid yielded a yellow solution, suggesting the presence of both Sn^{2+} and Sn^{4+} ions. The presence of Sn^{4+} ions diminishes the Sn^{2+} content, resulting in a less pronounced color change to white (**Figure 3(b)**). It can be concluded that $SnSO_4$ synthesized using 35 % sulfuric acid contains $Sn(SO_4)_2$ as an impurity. The iodine test results for powder produced from 40 % sulfuric acid did not change color (**Figure 3(c)**). This suggests that the tin oxidation number in the product is tin (IV), or Sn^{4+}. Sn^{4+} ions are not oxidized by iodine solution; thus, the color does not change. Based on the iodine test results, it can be concluded that the optimum concentration of sulfuric acid is 30 %, as it allows for the synthesis of pure $SnSO_4$ without the presence of $Sn(SO_4)_2$ impurity.

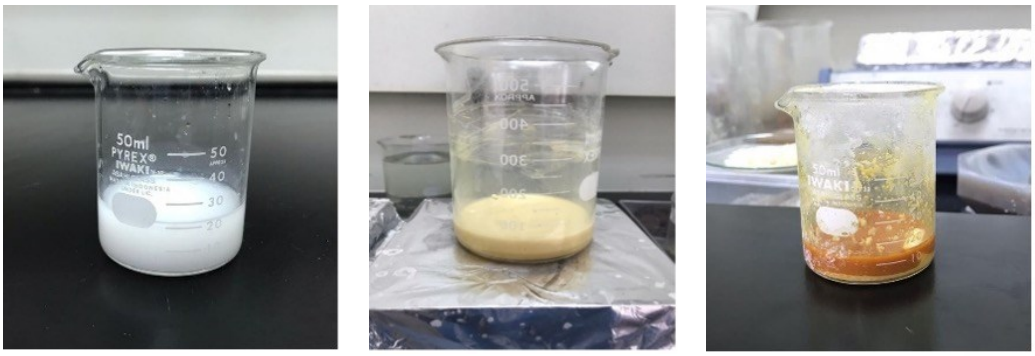

(a) (b) (c)

Figure 3 Iodine discoloration test results on synthetic powder using; (a) 30 %; (b) 35 %; and (c) 40 % sulfuric acid.

In addition to the iodine test, the thermal activity of the synthesized powders was evaluated using Differential Thermal Analysis (DTA). A sample of 0.2 g of powder was subjected to a heating rate of 2.5 °C/min from 25 to 950 °C. According to the test results, the DTA intensity for powder synthesized using 30% sulfuric acid and commercial $SnSO_4$ coincides at ~558 °C, with values of 0.108 and 0.115, respectively (**Figures 4(a)** and **4(b)**, red circles). This DTA data suggests that within this temperature range, $SnSO_4$ decomposes into SnO_2 and SO_2, as indicated by Eq. (5) on **Table 1**.

The powder synthesized using 35 % sulfuric acid exhibited a peak at ~700 °C with an intensity of 0.9246. According to Ahmed's previous research, this peak confirms the presence of both $SnSO_4$ and $Sn(SO_4)_2{\cdot}4H_2O$ [10], This is because $Sn(SO_4)_2{\cdot}4H_2O$ decomposes to SnO_2 and SO_3, as depicted by Eq. (9) on **Table 1**. The DTA results for the powder synthesized using 40 % sulfuric acid further confirmed the formation of $Sn(SO_4)_2{\cdot}4H_2O$, as evidenced by the DTA graph showing peaks at 550 and 700 °C with intensities of 0.5876 and 0.5904, respectively (**Figure 4(a)** and **4(b)**, green boxes). Both $SnSO_4$ and $Sn(SO_4)_2{\cdot}4H_2O$ were produced, with peak ~550 °C corresponding to the decomposition of $SnSO_4$ into SnO_2 and SO_2 (Eq. (5)) and peak ~700 °C representing the decomposition of $Sn(SO_4)_2{\cdot}4H_2O$ into SnO_2 and SO_3 (Eq. (9)). The formation of $Sn(SO_4)_2{\cdot}4H_2O$ should be avoided as it is difficult to separate from $SnSO_4$. Based on the DTA results, the DTA intensity for powder synthesized using 30 % sulfuric acid and $SnSO_4$ commercial are identical, while the powder synthesized using 35 and 40 % sulfuric acid exhibited a peak confirms the presence of both $SnSO_4$ and $Sn(SO_4)_2{\cdot}4H_2O$, which means there is Sn^{4+} contaminant in the product and that is strictly avoided. These results align with the iodine test results; 30 % sulfuric acid is determined to be the optimal concentration for synthesizing $SnSO_4$. While the reaction rate increases with increasing sulfuric acid concentration [27], excessive concentrations lead to overoxidation of tin, resulting in the formation of tin (IV) or $Sn(SO_4)_2{\cdot}4H_2O$.

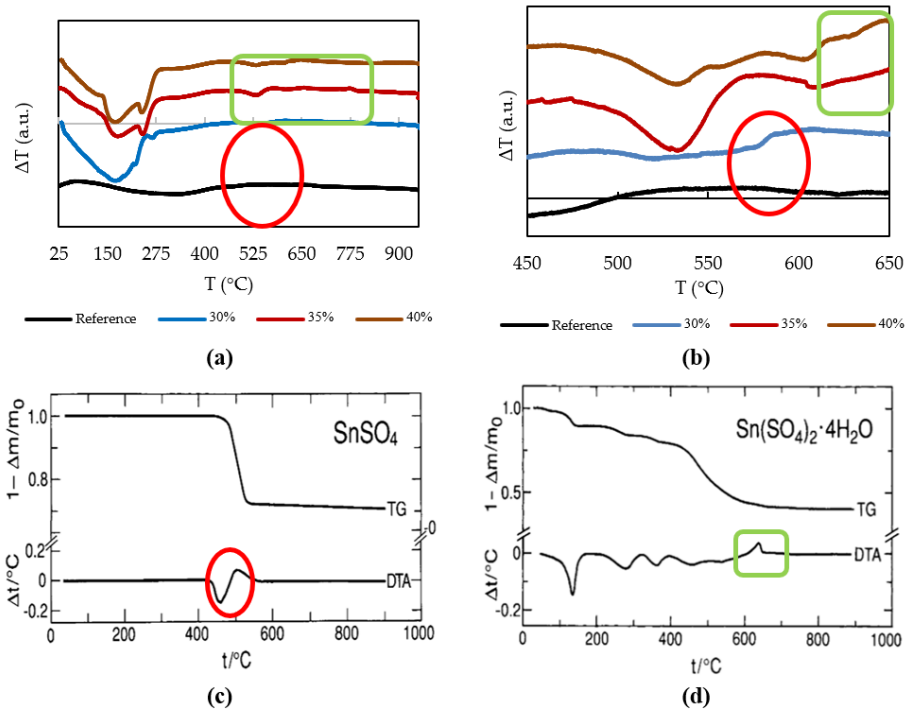

Figure 4 DTA results from synthesized powder at temperatures: (a) 25 - 950 °C; (b) 450 - 650 °C; and DTA Reference for: (c) $SnSO_4$; and (d) $Sn(SO_4)_2 \cdot 4H_2O$ [10].

Table 1 Summary of DTA results for reaction products [10].

Decomposition reaction	Equation	T (°C)	ΔT
$SnSO_{4\,(s)} \rightarrow SnO_{2\,(s)} + SO_{2(g)}$	(5)	558.7	0.11
$Sn(SO_4)_2 \cdot 4H_2O_{\,(s)} \rightarrow Sn(SO_4)_2 \cdot 2H_2O_{\,(s)} + 2H_2O_{\,(g)}$	(6)	171.6	–4.19
$Sn(SO_4)_2 \cdot 2H_2O_{\,(s)} \rightarrow Sn(SO_4)_2 \cdot H_2O_{\,(s)} + H_2O_{\,(g)}$	(7)	308.1	–1.39
$Sn(SO_4)_2 \cdot H_2O_{\,(s)} \rightarrow Sn(SO_4)_{2\,(s)} + H_2O_{\,(g)}$	(8)	384.3	0.37
$Sn(SO_4)_{2\,(s)} \rightarrow SnO_{2\,(s)} + 2SO_{3(g)}$	(9)	656.3	1.15

Based on the iodine discoloration and DTA tests results, it is known that 30 % sulfuric acid is the optimum concentration of sulfuric acid. The role of concentration is foremost to synthesize $SnSO_4$. Since the optimum concentration is obtained, the next step is to determine the optimum heating temperature and reaction time to obtain the most efficient approach to synthesize $SnSO_4$.

Effect of heating temperature on the synthesis of tin (II) sulphate ($SnSO_4$)

Having established the optimal sulfuric acid concentration, the focus shifted to determining the most efficient heating temperature for $SnSO_4$ synthesis. Previous studies have employed heating temperatures between 50 - 95 °C for 5 to 30 days, but these methods are time-consuming [10,18]. This was attributed to the slow reaction kinetics at lower temperatures. Given that $SnSO_4$ synthesis involves an oxidation process, increasing the heating temperature can significantly accelerate the reaction [28]. As a result, the range of heating temperatures was expanded to 120, 150, 180 and 200 °C.

In this study, tin was reacted with stoichiometrically proportionate 30 % sulfuric acid at each of the specified temperatures for 2 h. Following the synthesis process, the oxidation state of tin in the resultant powder was evaluated using both the iodine test and DTA. The iodine test results indicated a color change from brown to white, as seen in **Figure 5**. This transformation signified the successful synthesis of $SnSO_4$ powder at 120, 150 and 180 °C.

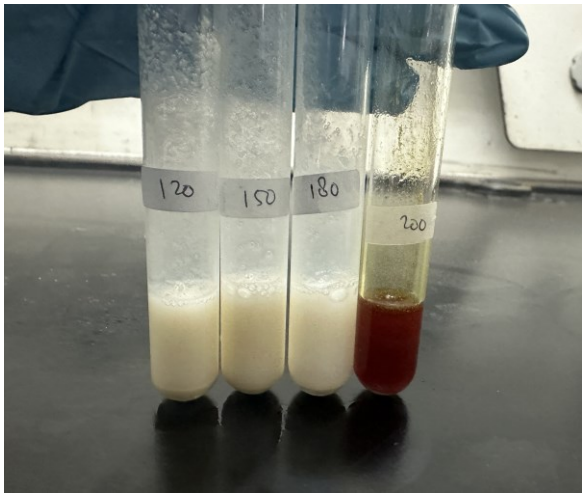

Figure 5 Iodine discoloration test results on synthetic powder at temperatures: 120, 150, 180 and 200 °C.

Furthermore, the synthesis powder was subjected to thermal activity analysis using Differential Thermal Analysis (DTA). The DTA spectra revealed that the powders synthesized at 120, 150 and 180 °C exhibited similar thermal profiles to commercial $SnSO_4$. However, the powder synthesized at 200 °C displayed a peak at ~736 °C with an intensity of 1.795, as depicted in **Figures 6(a)** and **6(b)** (green boxes). This peak corresponds to the decomposition of $Sn(SO_4)_2 \cdot 4H_2O$ into SnO_2 and SO_3, as indicated by Eq. (9) on **Table 1**.

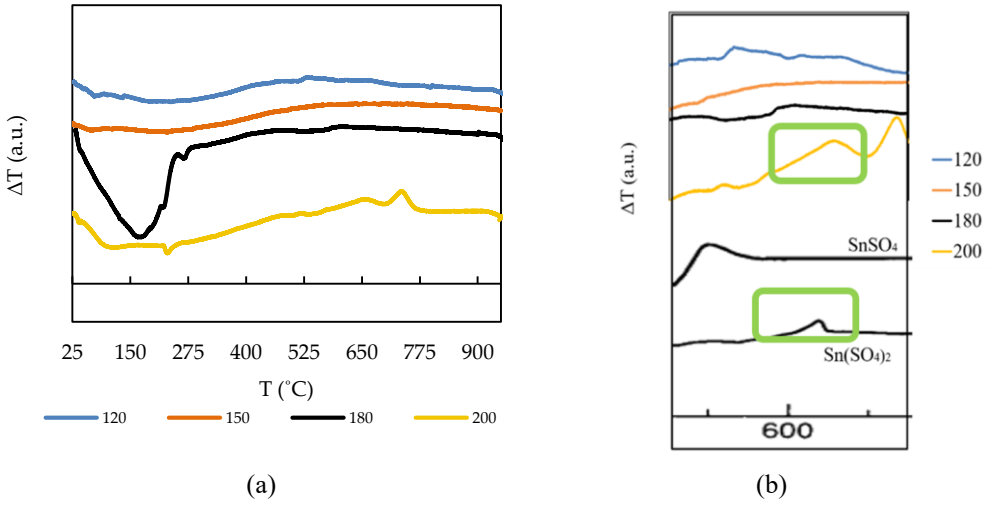

Figure 6 Thermal differential signal from the Differential Thermal Analyzer at several heating temperatures, with (a) complete signal (b) signal from 450 - 750 °C to compare the synthesized $SnSO_4$ with the reference from [10].

Considering that the synthesis processes conducted at 120, 150 and 180 °C yielded $SnSO_4$, the optimum heating temperature was determined based on the maximum yield achieved. **Figure 7** illustrates the amount of $SnSO_4$ produced at each temperature. Tin powder generated at 180 °C exhibited the highest yield, amounting to 45.89 g with a yield of 96.4 %. Consequently, a temperature of 180 °C was established as the optimal heating temperature for synthesizing $SnSO_4$.

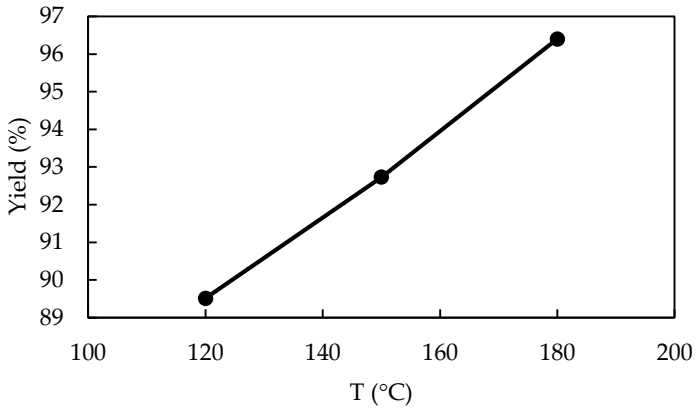

Figure 7 Yield of $SnSO_4$ produced at temperatures of 120, 150 and 180 °C.

Effect of reaction time on the synthesis of tin (II) sulphate ($SnSO_4$)

With the optimal heating temperature established, the next step was to determine the optimal reaction time. Determining the ideal reaction time is crucial for optimizing the synthesis process. To ascertain the optimum reaction time, $SnSO_4$ synthesis was conducted using varying reaction times and evaluated using both the iodine test and DTA. **Figures 8(a)** and **8(b)** demonstrates that $SnSO_4$ was successfully synthesized using 30 % sulfuric acid for 1 and 2 h, as evidenced by the iodine test, where the solution color transformed into a white solution. On the other hand, the synthetic processes conducted for 3 and 4 h exhibited a partial color change, shifting from brown to light brown (**Figures 8(c)** to **8(d)**). This indicates that the reaction did not fully proceed, resulting in incomplete synthesis of $SnSO_4$. Furthermore, the iodine test results for the synthetic powder subjected to 5 and 6 h of reaction (**Figures 8(e)** and **8(f)**) suggest incomplete synthesis, with the solution retaining a brown color. Therefore, it can be concluded that $SnSO_4$ synthesis can be achieved effectively within the 1 and 2-hour timeframe.

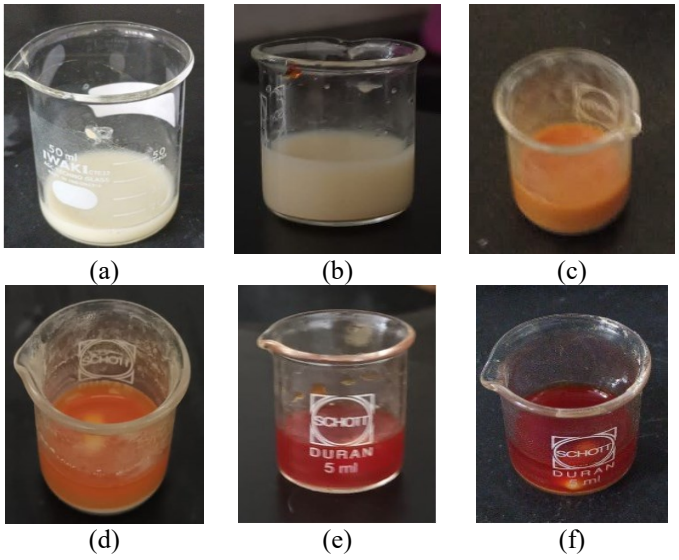

Figure 8 Iodine test results on synthetic powder for (a) 1; (b) 2; (c) 3; (d) 4; (e) 5; and (f) 6 h.

The DTA results (**Figure 9**) align with the iodine test findings. Reaction times of 1 and 2 h exhibit a single peak in the range 450 - 600 °C (marked in red circles). These peaks are attributed to the decomposition of $SnSO_4$ into SnO_2 and SO_2, as indicated by Eq. (5) on **Table 1**. In contrast, **Figure 9(b)** reveals the presence of an additional peak in the 300 - 700 °C range for reaction times of 3, 4, 5 and 6 h. This peak, indicated by green boxes, corresponds to the decomposition of $Sn(SO_4)_2 \cdot 4H_2O$ into SnO_2 and SO_3, as per reference literature [10]. To determine the optimum reaction time, the yield of each synthesized

powder was assessed. A reaction time of 2 h yielded the largest amount of $SnSO_4$, namely 45.85 g with a yield of 96.3 %wt. Consequently, the optimum reaction time for synthesizing $SnSO_4$ is established as 2 h.

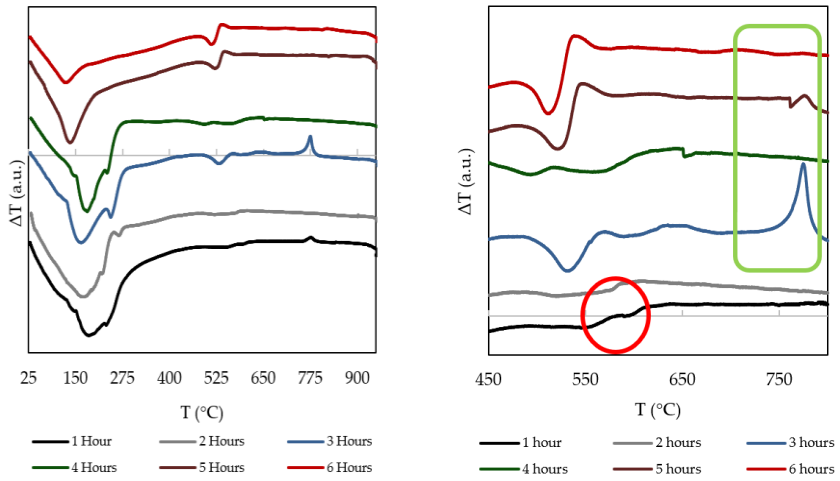

(a) (b)

Figure 9 DTA test results for determining Optimum reaction time with (a) temperature range 25 - 950 °C and (b) temperature range 450 - 800 °C.

Oxygen role on the Synthesis of Tin (II) sulphate ($SnSO_4$)

The next phase involved determining the role of oxygen in the synthesis process. To investigate this, a blank procedure was carried out in which tin powder was reacted with 30 % sulfuric acid, but without the presence of oxygen. The results revealed that the absence of oxygen prevented the formation of the intermediate compound SnO and instead, the tin powder reacted directly with the sulfuric acid to form tin (IV). This was confirmed by both the iodine test and DTA analysis. The iodine test showed that the solution remained brown, indicating the presence of tin (IV) in the synthesized product (**Figure 10**). The DTA analysis also demonstrated that the synthesized powder exhibited a peak at ~656 °C with an intensity of 1.15, which corresponds to the decomposition of $Sn(SO_4)_2$ to SnO_2 and SO_3 (**Figure 11**), with some trace peaks corresponded to hydrate molecules release. Our finding in a good agreement with some previous studies. Richter *et al.* [18] highlighted the dependency of $SnSO_4$ synthesis on the presence of oxygen [18]. This aligns with the findings of Mori and team, indicating that pure tin does not readily dissolve in oxidizing agents devoid of acid. However, the formation of Sn^{2+} ions is contingent upon the dissolution of tin in sulfuric acid that is saturated with oxygen [27-29].

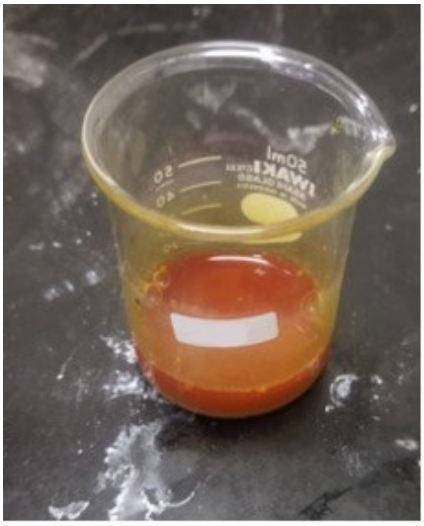

Figure 10 Iodine test results on synthetized powder without oxygen flow.

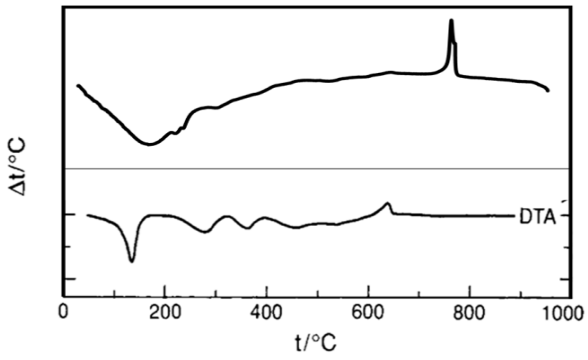

Figure 11 DTA results from blank powder stacked with DTA Reference for $Sn(SO_4)_2.4\ H_2O$.

The absence of oxygen in the synthesis process poses a significant challenge to the formation of $SnSO_4$ due to the unstable nature of SnO in oxygen-deficient environments. Studies have demonstrated that the formation of SnO is crucial for $SnSO_4$ synthesis, as it serves as a key precursor for the synthesis of $SnSO_4$ [18,32,30]. This is because SnO readily dissociates in the presence of oxygen, releasing oxygen atoms that can then react with Sn^{2+} ions to form $SnSO_4$ [32,33,36]. Previous studies have shown that the saturation of the oxygen coverage on Sn surfaces occurs upon exposure to 10 L of O_2 gas [22,33]. To ensure that oxygen was present throughout the synthesis process, oxygen gas was continuously flowed into the reaction chamber at a rate of 15 mL/s for 12 min. This allowed for the saturation of the tin surfaces with oxygen, ensuring that the reaction proceeded smoothly.

The oxidation process of tin by air initiates upon exposure to molecular oxygen, where dissociation chemisorption occurs and oxygen binds to surface tin atoms [20-22]. This mechanism involves either a trapping-mediated process or a direct chemisorption mechanism, the former requiring a 2-stage approach [22,33]. Eq. (10) illustrates the initial stage involving stable molecular oxygen:

$$O_2 + Sn \rightleftharpoons O_2*/Sn \quad (10)$$

This equation depicts an elongated oxygen bond compared to a free molecule, represented by O_2*, upon being trapped at the tin surface. Subsequently, oxygen may desorb into the gas phase or transition to a dissociative chemisorbed state, with rates influenced by surface temperature-mediated kinetics [22-25]. If not desorbed, the subsequent stage involves the activated transition of oxygen to a chemisorbed atomic state, where the O-O bond is disrupted and O atoms draw closer to the tin surface [22,33]:

$$O_2*/Sn + 2e^- \rightarrow 2O^-/Sn \quad (11)$$

In contrast, the direct mechanism portrayed in Eq. (11) exhibits the direct approach of oxygen molecules. Nevertheless, it is imperative to note that at the applied oxygen pressure, the duration required for the saturation of tin surfaces with dissociative chemisorbed oxygen atoms is expected to be significantly faster than the time resolution of applied ellipsometry measurements. Considering the applied oxygen flux, it is estimated that tin surfaces should attain saturation within approximately 1 s of O_2 exposure. Therefore, it is proposed that the initial oxide growth rate, as observed via ellipsometry, corresponds to the dissociation of molecular species on an oxygen-saturated surface, combined with the incorporation of oxygen atoms in sub-surface layers. This proposed mechanism is represented by Eq. (12):

$$O_2*/(SnO_{Surface} + Sn_{Sub\text{-}surface}) + e^- \rightarrow O^-/(SnO_{x\ Surface\ +\ SnOsub\text{-}suface}) \quad (12)$$

In instances where the molecular dissociation of O_2 on an oxygen-saturated surface acts as the limiting step for the initial oxide formation phase, it is suggested that the energy barrier for this process could be derived through Arrhenius analysis. Notably, the adsorption and dissociation of oxygen, along with the formation of a chemical bond with the metal surface, result from electron donation from the metal surface into the antibonding orbitals of the oxygen molecule [22,24]. Consequently, it is anticipated that the interaction with oxygen (and other adsorbents) should follow a pattern similar to that observed in calculations. While no prior quantitative analysis of molecular oxygen dissociation was conducted for initially polycrystalline metallic surfaces like those in our experiments, at least following surface saturation

with oxygen, comparisons with simulations [22,33,34] and experimental data on single-crystalline metals [22,34] support observed trends and differences in dissociation energy [22].

Miyamoto *et al.* [35] asserted that the rate of oxygen oxidation in the reaction is independent of the concentration of sulfuric acid. The calculated value can be regarded as an approximate measure of oxygen dissolution into sulfuric acid solution during the oxidation reaction. The dissolution rate of oxygen into sulfuric acid solution experiences a rapid decline with increasing sulfuric acid concentration [26,35].

To ensure the absence of any disproportionation process, oxygen continues to flow into the chamber throughout the synthesis process. The disproportionation reaction in Eq. (2) occurs spontaneously ($\Delta G°298 = -5.9$ kJ mol^{-1}) [22,30]. The lone pair in Sn^{2+} significantly influences the crystal chemistry of tin oxide. This compound, being tetragonal, comprises layers of tetragonal pyramids SnO_4 with Sn positioned apically. In Eq. (2), half of the Sn atoms are expelled from the solid framework at moderately mild temperatures. Tin's low melting point leads to considerable mobility, aiding the formation of liquid drops. Qualitative descriptions of the disproportionation of SnO remain limited in the literature.

The results, as per references, underscore the paramount importance of forming intermediate SnO in $SnSO_4$ synthesis. Despite kinetic reaction rates indicating the insignificance of oxygen oxidation compared to sulfuric acid, the absence of oxygen renders tin metal incapable of synthesizing $SnSO_4$ [28].

Characterization of the synthesized Tin (II) sulphate ($SnSO_4$)

Phase analysis of tin (II) sulphate ($SnSO_4$) produced

A comprehensive analysis of the XRD pattern in **Figure 12** unequivocally demonstrates the successful synthesis of $SnSO_4$, exhibiting a remarkable conformity with the standard reference. The XRD pattern of the synthesized sample furnishes compelling evidence of its purity, with no discernable impurities detected. **Figure 12** presents the XRD pattern of $SnSO_4$ meticulously prepared *via* the controlled flow of oxygen atmosphere into tin powder, followed by a reaction with 30 % sulfuric acid at an elevated temperature of 180 °C for an optimal duration of 2 h. This optimized preparation protocol resulted in $SnSO_4$ that closely matched the reference pattern (JCPDS No. 04-016-5779). All diffraction peaks in the XRD pattern can be unambiguously attributed to the characteristic (011), (002), (211), (202), (020) and (221) planes of $SnSO_4$, further solidifying the purity and authenticity of the synthesized material. Notably, the diffraction pattern for the synthesized $SnSO_4$ exhibited the highest peak at a 2θ value of around 25°, devoid of any contamination peaks. This remarkable absence of impurities underscores the impeccable purity of the synthesized $SnSO_4$. Moreover, the absence of additional diffraction peaks from another compound serves as an indicator of the single-phase nature of the synthesized $SnSO_4$.

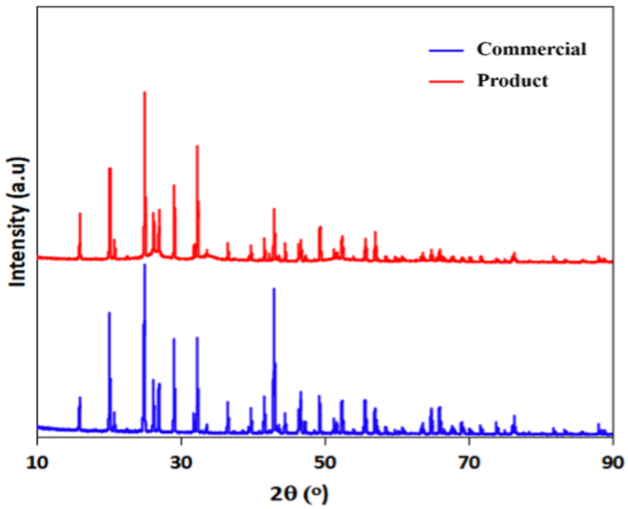

Figure 12 Comparison of the X-ray diffraction (XRD) of commercial tin (II) sulfate and tin (II) sulfate synthesized according to the present research.

To further elucidate the crystallinity and particle size characteristics of the synthesized $SnSO_4$, the XRD pattern provides crucial insights. The width of each diffraction peak serves as a direct reflection of the crystal size and its degree of crystallinity. Accordingly, the Scherrer equation, a well-established tool in crystallography, was employed to estimate the average crystal size (D) of $SnSO_4$:

$$D = \frac{K\lambda}{\beta \cos \theta} \quad (13)$$

where K represents the crystallite shape factor (K = 0.9), λ denotes the wavelength of X-ray radiation (λ = 1.5418 Å), β represents the full width at half maximum (FWHM) in radians and θ signifies the Bragg angle in degrees [36]. By substituting the relevant values from the XRD peak data into the Scherrer equation, an average crystal size of $SnSO_4$ of approximately ~666 nm was determined. This remarkable crystal size, coupled with the impeccable purity and single-phase nature of the synthesized $SnSO_4$, strongly validates the efficacy of the employed synthesis protocol.

Elemental analysis of Tin (II) sulphate ($SnSO_4$) produced

The composition of the synthesized product was meticulously analyzed using X-ray fluorescence (XRF) spectroscopy. The absence of significant impurities, evident from the XRF data (summarized in **Table 2**), further confirms the exceptional purity of the synthesized tin sulfate. The presence of only trace amounts of other elements corroborates the high level of purity achieved. This stringent purity regimen is essential for ensuring the desired properties and performance of the synthesized tin sulfate.

Table 2 Results of XRF Characterization of $SnSO_4$-synthetic and $SnSO_4$ -commercial.

Element	$SnSO_4$-reference		$SnSO_4$-Synthesis	
	Elemental Conc.	**Molecular Conc.**	**Elemental Conc.**	**Molecular Conc.**
$SnSO_4$	**-**	**98.568**	**-**	**98.369**
Sn	**92.997**	**-**	**87.256**	**-**
S	5.625	-	10.994	-
Cl	0.053	0.049	0.268	0.224
Ca	0.472	0.820	0.423	0.706
Cr	-	-	0.010	0.007
Mn	-	-	0.004	0.003
Fe	0.002	0.001	0.110	0.072
Ag	0.688	0.435	0.662	0.424
Pb	0.013	0.009	-	0.024
P	0.150	0.118	0.152	0.118
Pb	-	-	0.036	0.024
Sr	-	-	0.005	0.003
Eu	-	-	0.002	0.001
Ni	-	-	0.006	0.004
Zn	-	-	0072	0.047

Morphology, particle size and semi-quantitative elements analysis of Tin (II) sulphate ($SnSO_4$)

Figure 13 showcases the prismatic morphology of $SnSO_4$, characterized by uneven surfaces and irregular particle sizes. The synthesized $SnSO_4$ and its commercial counterpart exhibit similar prismatic shapes with varying particle sizes, as evident in **Figures 13(a)** and **13(b)**. Notably, the synthesized $SnSO_4$ exhibits a significantly smaller size compared to the commercial product. This observation is supported by the magnified images in **Figures 13(c)** and **13(d)**, where the synthesized $SnSO_4$ was imaged at 15,000x magnification, while the commercial product was imaged at 3,000x magnification. To quantify the average size of the synthesized $SnSO_4$, ImageJ software was employed. The analysis revealed that the average diameters of the synthesized $SnSO_4$ and the commercial product were 2.32 and 73.48 μm, respectively. Similarly, the average lengths of the synthesized $SnSO_4$ and the commercial product were determined to be 3.47 and 73.48 μm, respectively.

Figure 14 presents the elemental distribution pattern of the synthesized $SnSO_4$, revealing the presence of Sn, S and O through their characteristic emission peaks, as observed in **Figure 15** (Mα range from 0.5 - 4.5 keV). The distribution of those elements is also homogeneous throughout the particles, indicating strong evidence of $SnSO_4$. Interestingly, another trace element, discernible from the precursor tin powder, was also detected.

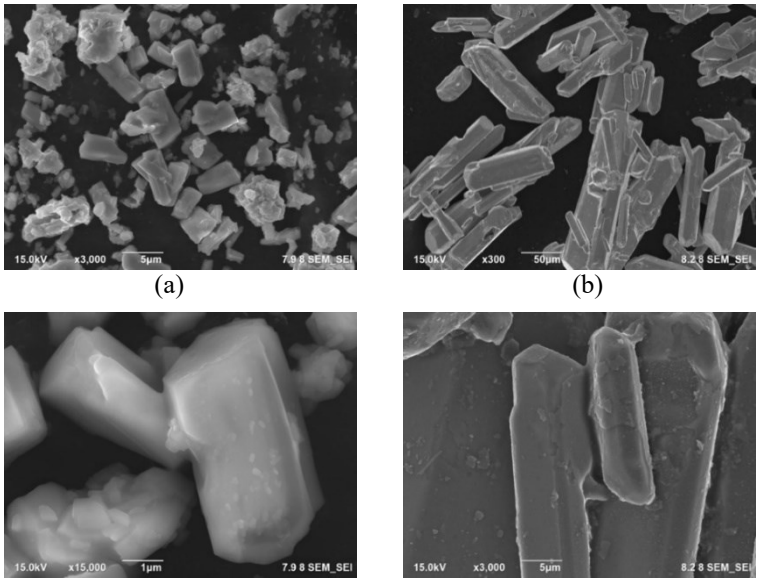

Figure 13 Comparison of the morphology of (a) $SnSO_4$ from synthesis at 3,000× magnification, with (b) commercial $SnSO_4$ at 300× magnification, (c) $SnSO_4$ from synthesis at 15,000× magnification and (d) commercial $SnSO_4$ at 3,000× magnification.

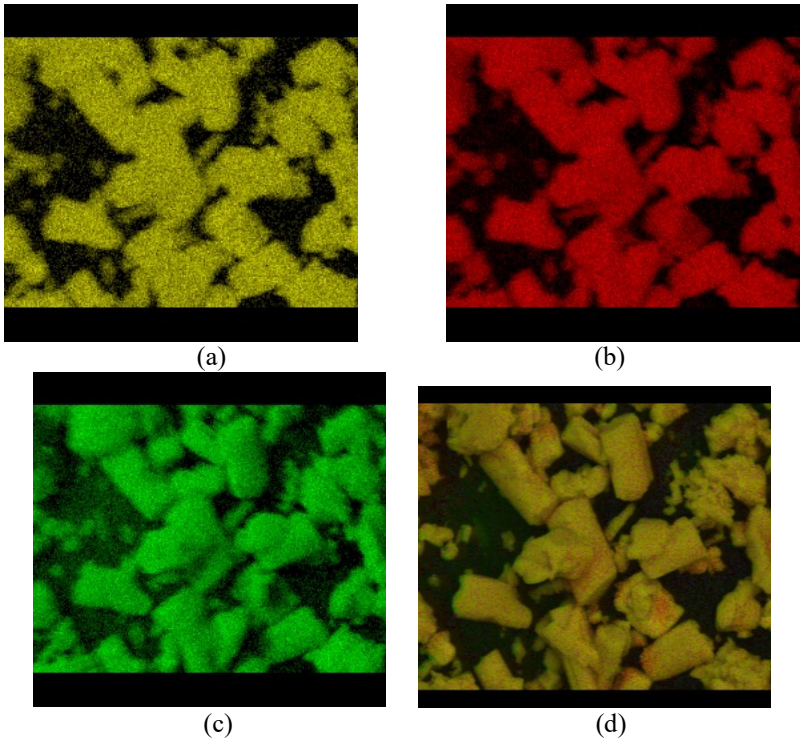

Figure 14 EDX image for synthesized $SnSO_4$ (a) mapping Sn; (b) Mapping S; (c) Mapping O; and (d) Mixed layer mapping.

To further scrutinize the structural characteristics of the synthesized $SnSO_4$, TEM was employed. **Figure 16(a)** presents a TEM image of the sample, revealing a distinctly different morphology compared to the SEM analysis. While SEM images displayed a prismatic structure, TEM revealed an irregular morphology. This discrepancy may be attributed to the beam-sensitive nature of $SnSO_4$, which suggests that the electron beam exposure may have altered the crystal structure.

To corroborate this hypothesis, selected area electron diffraction (SAED) was performed, as shown in **Figure 16(b)**. The SAED pattern revealed the presence of both amorphous and crystalline phases, indicating the potential beam-induced structural modification of $SnSO_4$. While some diffraction spots were observed, they did not fully represent the high crystallinity typically associated with $SnSO_4$. Despite the apparent beam sensitivity, the observed SAED pattern allowed for the indexing of the ring patterns, corresponding to the (202), (103), (323), (712) and (352) planes of the orthorhombic crystal system. This finding further supports the structural identity of $SnSO_4$, albeit with potential structural alterations induced by the electron beam exposure.

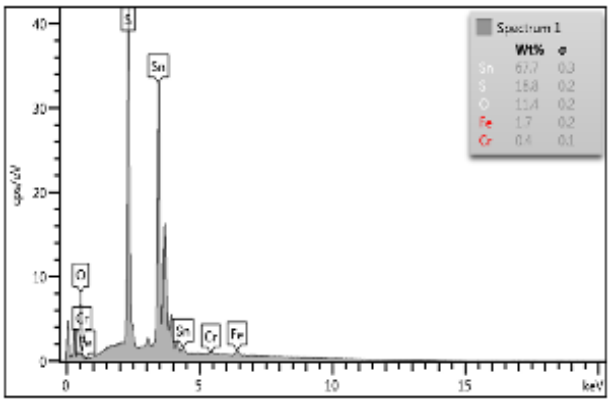

Figure 15 EDX spectrum of synthesized $SnSO_4$.

The STEM and HAADF-STEM images of the synthesized $SnSO_4$ further corroborate the presence of Sn, S and O elements in the synthesized product, providing compelling evidence of its chemical composition (**Figures 16(c)** to **16(d)**). These high-resolution imaging techniques enabled the visualization of individual Sn, S and O atoms within the $SnSO_4$ lattice structure, confirming the successful synthesis of the target compound.

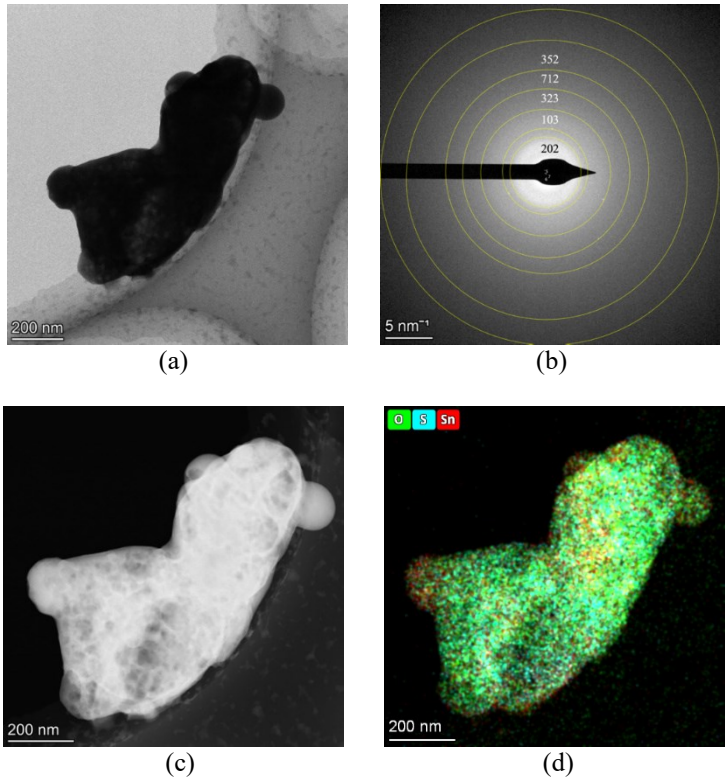

(a) (b)

(c) (d)

Figure 16 TEM images for (a) Morphology; (b) SAED; (c) STEM; and (d) SI HAADF-STEM image of synthesized $SnSO_4$.

In a brief conclusion, TEM analysis has unveiled the beam-sensitive nature of $SnSO_4$, potentially altering its crystal structure upon electron beam exposure. While the observed SAED pattern indicated the presence of both crystalline and amorphous phases, it did not fully capture the high crystallinity typically associated with $SnSO_4$. Further studies are warranted to elucidate the extent of beam-induced structural modifications and their impact on the material's properties.

Conclusions

Our study demonstrates showcases the efficient production of Tin (II) sulfate ($SnSO_4$) by employing 30 %wt sulfuric acid under a 180°C temperature for 2 h. These findings are congruent with both the results of the iodine discoloration test and thermal analysis. The obtained results reveal a prismatic morphology characterized by a singular phase, boasting a purity level of 98.369 %. A thorough analysis of the crystal and particle sizes revealed an average size of ~666 nm and 3.47 μm, respectively. These dimensions underscore the uniformity and consistency of the synthesized $SnSO_4$ crystals. The presence of oxygen during the reaction proved to be a pivotal factor in the successful synthesis of $SnSO_4$. Under an oxygen-rich environment, tin (II) ion formation is facilitated, leading to the formation of the desired $SnSO_4$ compound. Conversely, in the absence of oxygen, the tin (II) ions undergo further oxidation to form undesirable tin (IV) oxide, thereby altering the desired product composition.

Acknowledgements

The authors would like to thank National Research and Innovation Agency through Rumah Program of Nanotechnology and Advanced Materials (Grant number: 13/ III.10.1/HK/2023 Code: 145), Research Collaboration Center for Tin Metal (Grant number: 2534 /II.7/HK.01.00/5/2023) and Nanotechnology and Materials Research Organization (ORNM)- National Research and Innovation Agency (BRIN) on Research and Innovation Program for Advanced Indonesia Round 3 2023 [RIIM-3026157348] to fund this research. This research is also partly funded by Degree by research scheme of BRIN and characterization of facilities of National Research and Innovation Agency E-Science Services.

References

[1] J Pearce and T Wallace. *Tin chemicals roadmap 2015: Challenged but growing.* ITRI Ltd., Hertfordshire, 2015, p. 1-17.
[2] K Yim, Y Youn, M Lee, D Yoo, J Lee, SH Cho and S Han. Computational discovery of p-type transparent oxide semiconductors using hydrogen descriptor. *NPJ Comput. Mater*. 2018; **4**, 17.
[3] Q Wang, J Liu, D Yang, X Yuan, L Li, X Zhu, W Zhang, Y Hu, X Sun, S Liang, J Hu, RV Kumar and J Yang. Stannous sulfate as an electrolyte additive for lead acid battery made from a novel ultrafine leady oxide. *J. Power Sourc*. 2015; **285**, 485-92.
[4] M Nagayama, T Morita, H Ikuta, M Wakihara, M Takano and S Kawasaki. A new anode material $SnSO_4$ for lithium secondary battery. *Solid State Ionics* 1998; **106**, 33-8.
[5] MF Shaffei, HS Hussein, N Khatab, AM Awad, NA Shabaan and MS Shalaby. A comparative study for selecting more efficient black selective coating in solar water heating system. *Egypt. J. Chem.* 2021; **64**, 5957-62.
[6] E Ovodok, M Ivanovskaya, D Kotsikau, V Kormosh, P Pylyp and V Bilanych. Structural characterization and gas sensing properties of nano-sized tin dioxide material synthesized from tin(II) sulfate. *Ukr. J. Phys.* 2021; **66**, 803-10.
[7] CO Pereira, MF Portilho, CA Henriques and FMZ Zotin. $SnSO_4$ as catalyst for simultaneous transesterification and esterification of acid soybean oil. *J. Braz. Chem. Soc.* 2014; **25**, 2409-16.
[8] CA Tajuddin, MI Amal, WB Widayatno, N Wulandari, DFD Purnomo and M Nasikin. Stannous chloride ($SnCl_2$) and stannous sulfate ($SnSO_4$) synthesis from tin powderization waste. *IOP Conf. Ser. Earth Environ. Sci.* 2021; **749**, 012025.
[9] COP Teixeira, KCNR Pedro, TLAP Fernandes, CA Henriques and FMZ Zotin. Esterification of high acidity vegetable oil catalyzed by tin-based catalysts with different sulfate contents: contribution of homogeneous catalysis. *Chem. Eng. Commun.* 2019; **206**, 169-81.
[10] MAK Ahmed, H Fjellvåg and A Kjekshus. Synthesis and characterization of tin sulfates and oxide sulfate. *Acta Chem. Scand.* 1998; **52**, 305-11.
[11] E Ruf and H Loges. 1978, Process for producing tin (II) sulfate, Canada Patent CA1106798A.
[12] LD Riese-Meyer, H Beaujean, J Bode, J Sander and V Sander. 1995, Manufactured tin (II) sulfate granules for electrolytic coloring with metal salts, Canada Patent CA2111869A1.

[13] WD Wüst, J Wollmann and DD Brodalla. 1989, Process for the preparation of tin II sulfate, Canada Patent EP0351550A1.
[14] C Zhen, C Riyao and W Ying. 1996, Producing method for stinnous sulfate, China Patent CN1124231A.
[15] S Rathore, H Madhav and G Jaiswar. Efficient nano-filler for the phase transformation in polyvinylidene fluoride nanocomposites by using nanoparticles of stannous sulfate. *Mater. Res. Innovat.* 2019; **23**, 183-90.
[16] X Yao, B Zhang, S Cui, S Yang and X Tang. Fabrication of $SnSO_4$-modified TiO_2 for enhance degradation performance of methyl orange (MO) and antibacterial activity. *Appl. Surf. Sci*. 2021; **551**, 149419.
[17] FC Mathers and HS Rothrock. Preparation of Stannous Sulfate. *Ind. Eng. Chem.* 1931; **23**, 831-2.
[18] H Richter and NJ Rahway. 1955, Manufacture of stannous sulfate from tin and sulfuric acid. US Patent US2726929A.
[19] SK Ali, H Wani, C Upadhyay, KSSNS Madhur, I Khan, S Gul, N Jahan, F Ali, S Hussain and K Azmi. Synthesis of CdS nanoparticles by chemical co-precipitation method and its comparative analysis of particle size via structural and optical characterization. *Indones. Phys. Rev.* 2020; **3**, 100-10.
[20] KR Lawless. The oxidation of metals. *Rep. Prog. Phys.* 1974; **37**, 231-316.
[21] AT Fromhold. *Theory of metal oxidation*. *In*: H Schmalzried (Ed.). Berichte der Bunsengesellschaft für physikalische chemie. North Holland Publishing, Amsterdam, 1976, p. 547.
[22] CRSV Boas, JM Sturm, WTEVD Beld and F Bijkerk. Oxidation kinetics of transition metals exposed to molecular and atomic oxygen. *Materialia* 2021; **20**, 101203.
[23] MC Wheeler, DC Seets and CB Mullins. Kinetics and dynamics of the initial dissociative chemisorption of oxygen on Ru(001). *J. Chem. Phys*. 1996; **105**, 1572-83.
[24] PD Nolan, MC Wheeler, JE Davis and CB Mullins. Mechanisms of initial dissociative chemisorption of oxygen on transition-metal surfaces. *Acc. Chem. Res*. 1998; **31**, 798-804.
[25] BA Ferguson, CT Reeves and CB Mullins. Oxygen adsorption on Si(100)-2x1 via trapping-mediated and direct mechanisms. *J. Chem. Phys*. 1999; **110**, 11574-84.
[26] S Miyamoto. On the oxidation of stannous chloride in sulphuric acid solution by air and the dissolution velocity of oxygen into Sulphuric acid solution. *Bull. Chem. Soc. Jpn*. 1928; **3**, 48-56.
[27] M Pourbaix, H Zhang and A Pourbaix. Presentation of an Atlas of chemical and electrochemical equilibria in the presence of a gaseous phase. *Mater. Sci. Forum* 1997; **251-254**, 143-8.
[28] M Mori, K Miura, T Sasaki and T Ohtsuka. Corrosion of tin alloys in sulfuric and nitric acids. *Corrosion Sci*. 2002; **44**, 887-98.
[29] FW Burry and JR Partington. CCXXXIX.- Preparation and reactions of stannous hydroxides. *J. Chem. Soc., Trans.***,** 1922**,121,** 1998-2004
[30] MS Moreno, G Punte, G Rigotti, RC Mercader, AD Weisz and MA Blesa. Kinetic study of the disproportionation of tin monoxide. *Solid State Ionics* 2001; **144**, 81-6.
[31] JH Hildebrand and BL Glascock. The color of iodine solutions. *J. Am. Chem. Soc*. 1909; **31**, 26-31.
[32] M Taguchi, J Kurihara and T Ishikawa. Reductive behaviour of oxidizing agents on the surface passive titanium in sulfuric acid solution. *Boshoku Gijutsu* 1988; **37**, 354-60.
[33] ED German and M Sheintuch. Relationship between kinetic and thermodynamic characteristics of oxygen dissociative adsorption on close-packed metal surfaces. *J. Phys. Chem. A* 2005; **109**, 7957-66.
[34] MM Montemore, MAV Spronsen, RJ Madix and CM Friend. O_2 activation by metal surfaces: implications for bonding and reactivity on heterogeneous catalysts. *Chem. Rev*. 2018; **118**, 2816-62.
[35] S Miyamoto. The rate of oxidation of stannous salt by oxygen and the electrical conductivity of mixtures of sulfuric acid and stannous sulphate. *Bull. Chem. Soc. Jpn*. 1932; **7**, 56-68.
[36] A Hermawan, Y Asakura, M Inada and S Yin. One-step synthesis of micro-/mesoporous SnO_2 spheres by solvothermal method for toluene gas sensor. *Ceram. Int*. 2019; **45**, 15435-44.